

## Lasing from Dot-in-Rod Nanocrystals in Planar Polymer Microcavities

Giovanni Manfredi,<sup>a†</sup> Paola Lova,<sup>a</sup> Francesco Di Stasio,<sup>b††</sup> Prachi Rastogi,<sup>b</sup> Roman Krahné,<sup>b</sup> and Davide Comoretto<sup>a\*</sup>

<sup>a</sup>Dipartimento di Chimica e Chimica Industriale, Università di Genova, Genova, Italy

<sup>b</sup>Nanochemistry Department, Istituto Italiano di Tecnologia, Genoa, Italy

<sup>†</sup>Present Address: Center for Nano Science and Technology, Istituto Italiano di Tecnologia, Milano, Italy.

<sup>††</sup>Present address: ICFO - The Institute of Photonic Sciences, Castelldefels (Barcelona), Spain

\*davide.comoretto@chimica.unige.it

---

### SUPPORTING INFORMATION

---

### S1. CdSe/CdS Dot-in-Rod size distribution:

Figure S1a reports a TEM image of the DiRs used in this work. The size distribution in length and diameter of the DiRs is shown (b). The histograms were obtained by TEM image analysis of 100 DiRs. The average size together with the standard deviation of the distribution are also reported.

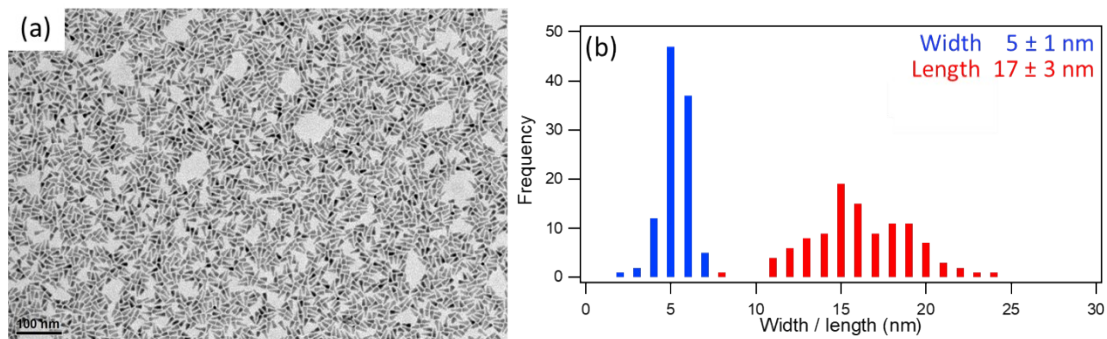


Figure S1: (a) TEM image of DiRs used in this study. (b) Histograms showing statistics of the DiR length (in red) and diameter (in blue).

## S2. Dot-in-Rod film homogeneity:

Since the DiRs are deposited by drop casting, the obtained film does not display the same homogeneity as those prepared in polymer nanocomposites (see ref.<sup>1</sup>). The film morphology can be evaluated by confocal PL imaging of the DiRs layer (Figure S2a and b). The fluorescence images were recorded with a NIKON A1 confocal microscope with a 10x objective, under excitation with a laser at 402 nm. The emission was detected in the range from 590-650 nm. From the xyz scan in Figure S2c we can estimate the thickness of the cavity layer to be around 5-10  $\mu\text{m}$ .

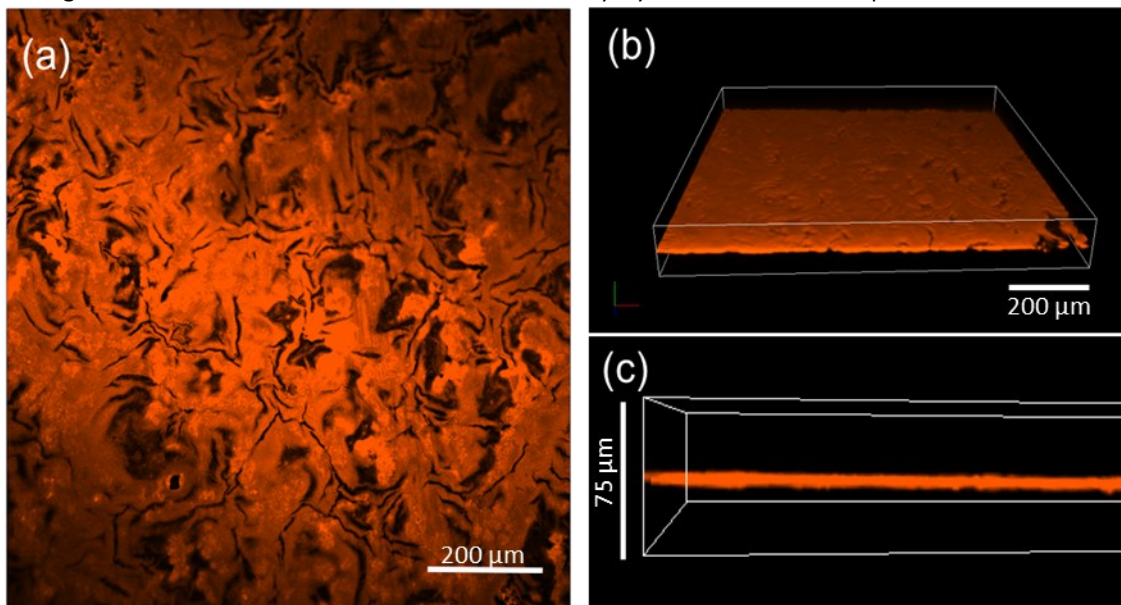


Figure S2: Confocal fluorescence microscopy images of the DiRs film recorded from a reopened microcavity. (a) Top view, (b-c) 3D representation of stacked images recorded in a xyz scan at different viewing angles. Scale bars correspond to 200  $\mu\text{m}$  in (a-b), and to 75  $\mu\text{m}$  in (c).

### S3. Spectral comparison of the DiRs PL:

In Figure S3a we compare the normalized emission spectra of the DiR reference film under CW and fs excitation. The signal acquired for the CW spectrum (in black) is reported as measured and normalized. The PL spectrum recorded under fs excitation has been filtered using a Savitzky-Golay filter and then normalized. The PL under fs excitation is 6 nm redshifted compared to CW excitation. The FWHM of both emission peaks is 27 nm.

In Figure S3b we compare the PL of the DiR reference film and of the microcavity under CW excitation and collection in the same conditions. The microcavity PL intensity is reduced for shorter wavelengths while is slightly increased at longer wavelengths.

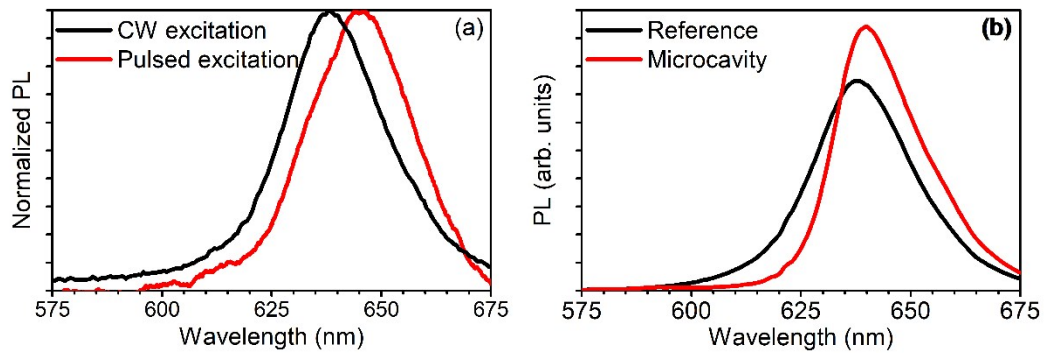


Figure S3: (a) Normalized PL of the DiRs film under CW (black) and pulsed fs excitation (red). (b) PL of the reference DiRs film (black) and microcavity (red) under CW excitation.

#### S4. Fluence dependence of emission in regions that do not show lasing

Given the inhomogeneity of the DiRs film, there are regions of the sample where no lasing is observed. In these regions, the emission spectrum is a non-trivial convolution of the PBG with the emission of the DiRs film. Figure S4a reports fs emission spectra from one of such regions measured for different fluences. For low excitation fluence, we can observe the long wavelength tail of the DiRs <sup>2</sup>emission, which extends further than the spectral range of the PBG. With increasing fluence this signal increases and, for fluences larger than 110  $\mu\text{J}/\text{cm}^2$ , a sharp high energy shoulder appears at 640 nm. This shoulder can be related to the spectrally cut-off ASE of the DiRs film. We notice that the threshold of the sharp high-energy shoulder relates well to the ASE threshold reported in Figure 2 of the main text. Therefore, we assign this peak to filtered ASE by the PBG of the microcavity.

Surprisingly, at much higher fluence (larger than 400  $\mu\text{J}/\text{cm}^2$ ), a peak at the short wavelength side of the PBG (centered at 594 nm) arises and strongly gains in intensity with increasing fluence. This spectral range lies outside the ASE and PL band of the DiRs emission. The emission peak at 595 nm corresponds to the second peak in the absorption spectrum of the DiRs film (see Figure 1 in main text), hence we tentatively assign it to higher energy optical transitions. In this scenario, we can suppose that the PBG of the microcavity stimulates transfer of oscillator strength from the band edge emission to such higher energy transitions, which enables PL and even ASE at these wavelengths.

The fluence dependence of PL at different wavelengths (595, 640 and 660 nm) is reported in Figure S4b. These wavelengths are representative of different physical effects: 660 nm labels the response of PL of the DiRs (similarly to the reference film), 640 nm corresponds to peak emission of the microcavity and the ASE wavelength, and 595 nm represents the peak which is spectrally positioned outside of the PBG. The response of the bare DiRs reference film is linear in the investigated fluence range. At 640 nm, the increase of the signal is linear (with slope 10.2 counts  $\text{cm}^2 \mu\text{J}^{-1}$ ) up to about 320  $\mu\text{J}/\text{cm}^2$ , then it saturates. Instead, the high-energy part of the emission initially increases with a slope that is comparable to the PL at 660 nm, while, at about 400  $\mu\text{J}/\text{cm}^2$ , its rises with a much steeper slope of 4.8 counts  $\text{cm}^2 \mu\text{J}^{-1}$ . This behavior suggests PL from higher energy transitions at low fluence that turn into ASE when excitation fluence exceeds 400  $\mu\text{J}/\text{cm}^2$ . Similar ASE from higher energy transitions has been observed from giant shell nanocrystals.<sup>2</sup>

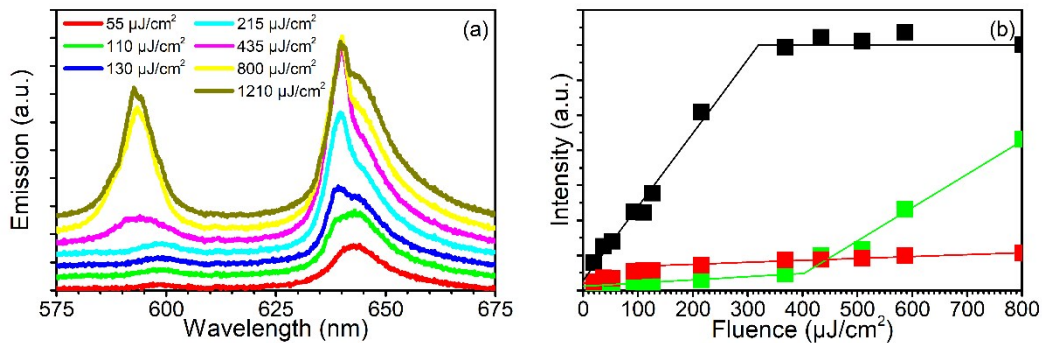


Figure S4: (a) fs PL spectra recorded from the microcavity as a function of pumping fluence from a region that does not manifest lasing; (b) Emission intensity at different wavelengths as a function of the pumping fluence (594 nm, high energy PL, in green; 640 nm, corresponding to the microcavity PL maximum, in black; 660 nm, related to the bare DiRs PL, in red).

## S5. Lasing from the microcavity and cavity thickness:

Figure S5 reports sample emission spectra under fs excitation from a spot showing lasing. The spectra are the same reported in Figure 4a in the main text, but the scale is magnified in order to better appreciate the multipeak structure at lower fluences.

The multipeak structure is created by the spectral modulation of the PL induced by the resonator. We can treat the microcavity as a Fabry-Perot etalon, where each peak is created by a resonator mode. Then, the optical length of the cavity can be estimated by the free spectral range, which is the difference in wavelength between the resonator modes. From Figure S5 we obtain the distance between neighboring peaks as  $\sim 2\text{nm}$ . Considering this as the free spectral range of the resonator  $\Delta\lambda_{fsr}$ , we can then estimate the cavity optical length ( $d$ ) from:<sup>3, 4</sup>

$$\Delta\lambda_{fsr} = \frac{\lambda^2}{2nd} \quad (\text{S.1})$$

Being  $\lambda = 640\text{ nm}$  and  $\Delta\lambda_{fsr} = 2\text{ nm}$ , we obtain a optical length  $nd = 102\ \mu\text{m}$ . For a DiRs refractive index of 2.5,<sup>5</sup> we can then estimate a geometrical thickness of  $41\ \mu\text{m}$ . This value is much larger than what was measured with confocal fluorescence on the central region of the film (Figure S2). One plausible possibility is that this distance originates localized regions of thicker nanocrystal aggregates that act as spacers. We note that a similar cavity length was reported in ref. <sup>6</sup> for a comparable fabrication process.

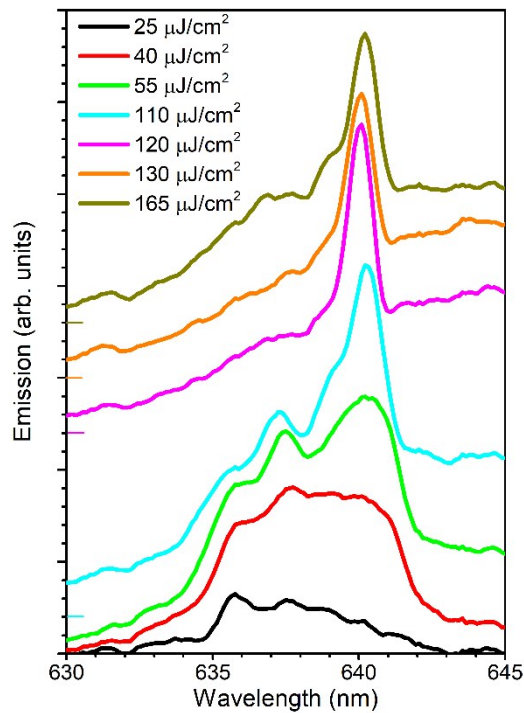


Figure S5: Stacked fs emission spectra of the microcavity collected perpendicularly to the sample for different pumping fluences. The spectra are the same as in Figure 4a of the main text but on a magnified scale.

### S6. Angular dependence of the emission of aged sample:

The emission from the microcavity has been examined after an aging of 18 months. The spectra as a function of pumping fluence can be examined in the main text. Figure S6 reports the emission spectra of the aged microcavity as a function of collection angle. The sample was pumped at  $3400 \mu\text{J}/\text{cm}^2$ , over the laser threshold. The reported angles are relative to the normal direction from the sample: the one perpendicular to the sample surface. For excitation up to  $4^\circ$ , we can clearly see a lasing peak at  $638 \text{ nm}$  over a broad PL background. For an angle of  $6^\circ$ , however, the lasing peak abruptly disappears leaving only the PL background. This measure clearly testifies the directionality of the lasing emission we measure from our sample.

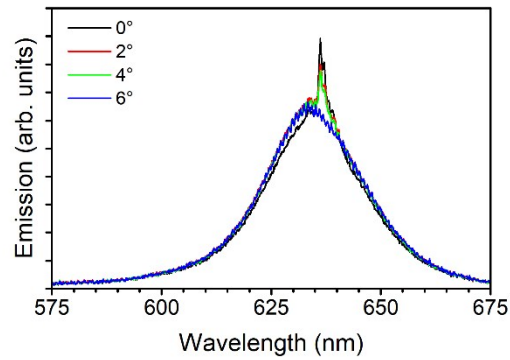


Figure S6: fs emission of the microcavity after 18 months of aging. The emission has been collected pumping at  $3400 \mu\text{J}/\text{cm}^2$ , higher than the lasing threshold. The emission has been collected at different small angles from the normal direction to the sample surface.

## Supporting references

1. G. Manfredi, P. Lova, F. Di Stasio, R. Krahné and D. Comoretto, *ACS Photonics*, 2017, **4**, 1761-1769.
2. F. Di Stasio, A. Polovitsyn, I. Angeloni, I. Moreels and R. Krahné, *ACS Photonics*, 2016, **3**, 2083-2088.
3. O. Svelto, *Principles of Lasers*, Springer Science + Business Media, Inc., New York, 4th Edition edn., 1998.
4. E. Hecht, *Optics*, Addison-Wesley, San Francisco, 2002.
5. I. Angeloni, W. Raja, R. Brescia, A. Polovitsyn, F. De Donato, M. Canepa, G. Bertoni, R. Proietti Zaccaria and I. Moreels, *ACS Photonics*, 2016, **3**, 58-67.
6. J. Q. Grim, S. Christodoulou, F. Di Stasio, R. Krahné, R. Cingolani, L. Manna and I. Moreels, *Nat. Nanotechnol.*, 2014, **9**, 891-895.